Stability and Bifurcation of Mathieu-Duffing Equation

Mohsen Azimi

Department of Aerospace and Mechanical Engineering, University of Arizona, Tucson, Arizona, 85721, USA

Abstract

Various phenomena in science, physics, and engineering result in the Mathieu equation with cubic nonlinear term, known as the Mathieu-Duffing equation. In previous works, different perturbation methods have been used to investigate the stability and bifurcation of this equation in the vicinity of the first unstable tongue and for relatively small values of natural frequency. The primary goal of this paper is to adapt the Strained Parameters Method to investigate the stability and bifurcation associated with stability change around the second unstable tongue. In addition, this work shows that the Strained Parameters Method is able to obtain the same results previously obtained by other perturbation techniques with minimum computational effort. An inductive approach is used to express the multipliers of the transition curves and the location of the newborn equilibria as a function of the parametric frequency. Lastly, the Floquet theory and Poincaré map are used to validate the analytical results.

Keywords: Mathieu-Duffing equation, pitchfork bifurcation, subharmonic bifurcation, supercritical bifurcation, subrcritical bifurcation, parametric resonance

1. Introduction

The classical Mathieu equation is a special case of Hill's equation [1], which was first introduced by French mathematician Emile Leonard Mathieu in 1868.

Email address: azimimohsen@email.arizona.edu (Mohsen Azimi)

When Mathieu was attempting to do the modal analysis of a stretched membrane with elliptical clamped boundaries. The Mathieu equation also appears in many other engineering problems such as floating ships, railroad trains, charged particles in electromagnetic Paul trap, elastic systems under time-varying load, and many others. This equation is a linear homogeneous second order differential equation with periodic coefficient. It is known that the origin is the only equilibrium point of this equation, and for given initial conditions it has oscillatory solutions with complex characteristics. This general solution remains either bounded (stable) or unbounded (unstable), while the unbounded response is associated with the parametric resonance. Determining the parameters in which the solutions to this equation remain bounded has been a crucial task. Usually, the result of the stability analysis is represented graphically in a parameter plane known as the Ince-Strutt stability diagram, where the transition curves separate the stable region from the unstable regions (Arnold tongues). Numerical approaches like Floquet Theory [2] and Energy Method [3, 4], as well as analytical methods like the Method of Multiple Scales [5], Strained Parameters Method [6], Method of Averaging [7], Harmonic Balance Methods [2] and Homotopy Perturbation Method [8] are utilized to find the transition curves in the Ince-Strutt stability diagram. In general, the numerical methods can be used for large values of parametric force, while analytical methods are valid only for the small values of the parametric force.

Consequently, various extensions of the linear Mathieu equation with damping [2], quadratic nonlinearity [9], cubic nonlinearity [10], delay [11], fractional derivative [12], quasiperiodic excitation [13], coupling [14, 15], and external excitation [16] terms have been considered. The Mathieu equation with cubic nonlinear term is one of the many geometrical nonlinear cases that have been investigated. This equation is also referred as Mathieu-Duffing equation, associated with the cubic nonlinear term of the Duffing equation. The governing Mathieu equation with cubic nonlinearity describes the nonlinear behavior of several phenomena, specifically elastic systems under periodic load, like Melde string [17]. Many works have attempted to study the periodic motion [18], sta-

bility [19], bifurcation and chaotic behavior [20] of this equation. Under the influence of the cubic nonlinearity and for different combinations of the parameters, it has been shown that the number of the equilibrium points and the stability of the origin change. Namely, the method of Multiple Scale [2], Method of Averaging [11], Poincaré-Lindstedt method [21], and Lie Transform [22] have been used to demonstrate the occurrence of the bifurcation in the Mathieu-Duffing equation.

In general, the Method of Multiple Scale is the standard approach used to find the eigenvalues of the Jacobian matrix for the bifurcation analysis of the Mathieu-Duffing equation around the first unstable tongue [2]. In this paper, it is shown that the Strained Parameters Method can be used as an alternative, to replicate the same results. The main objectives of this work is to include higher other terms in the Strained Parameters Method for the bifurcation analysis of the Mathieu-Duffing equation around the second unstable tongue, and subharmonic bifurcation for relatively low values of natural frequency. This is mainly because including higher order terms in the Method of Multiple Scale, results in additional right-hand side terms, which adds up to the complexity of the perturbation analysis. Investigating the number, location, and stability of the new-born equilibria around the origin is the main target of this work, and the effect of newborn equilibria on the transient or steady-state responses (periodic or quasiperiodic) is not a concern. In this work, an inductive approach is used to utilize the Strained Parameters Method for deriving the newborn equilibria in the bifurcation diagram and transition curves in stability chart, all as a function of parametric frequency. This is while in the great majority of previous studies the value of the parametric frequency has been consider equal to constants one [2] or two [3]. Finally, numerical integrations are carried out in conjunction with Floquet theory and the Poincaré map to validate the analytical results.

The remainder of this paper is organized as follows: In section 2, a mechanical model for the linear Mathieu equation is represented and discussed. In section 3, the analytical calculation is shown, including the derivation of the transition curves for the linear Mathieu equation, and the creation and stability of the

equilibrium points for the Mathieu-Duffing equation. In section 4, the results of the numerical calculations are illustrated and compared to validate the analytical results obtained in section 3. The last section includes the conclusion and final remarks.

2. Modeling

Many mechanical and electrical systems are described by the Mathieu equation. The most popular mechanical model is a parametrically excited pendulum, known as the Kapitza pendulum [2, 20, 23], which is a planar pendulum composed of a massless rigid rod and a heavy small bob on its end with a pivoting point subjected to periodic motion in the vertical direction. A schematic of such a system is shown in Fig. 1.

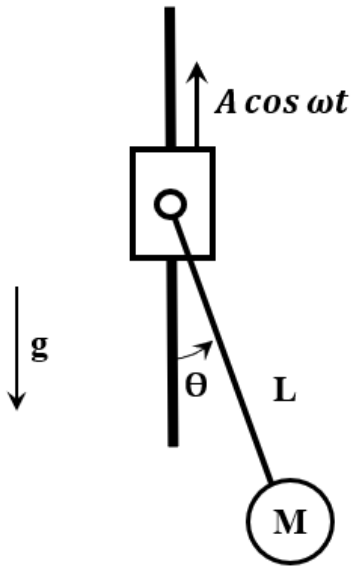

Figure 1: Kapitza Pendulum.

where θ is the generalized coordinate determining the angular displacement and constants M, g, L, A, and ω are the mass of the bob, gravity, length of the

rod, and the amplitude and frequency of the vertical motion, respectively. The governing differential equation of this system is provided below.

$$\ddot{\theta} + (\frac{g}{L} - \frac{A\omega^2}{L}\cos\omega t)\sin\theta = 0. \tag{1}$$

This equation has two equilibrium points at $\theta = 0$ and π. Taylor approximation can be used to write Eq. (1) in the following form, for the small values of θ, to study the local stability of each equilibrium point.

$$\ddot{\theta} \pm (\frac{g}{L} - \frac{A\omega^2}{L}\cos\omega t)\theta = 0, \tag{2}$$

where the positive and negative signs correspond to the equilibria at $\theta = 0$ and π, respectively. For the non-parametrically excited system, $\theta = 0$ and π are stable and unstable, respectively. Under parametric excitation and for different parametric frequencies the stability of both equilibrium points changes.

3. Analytical Calculations

In this work, the unperturbed nonlinear Mathieu equation with cubic nonlinear term and no damping is written in the following standard form.

$$\ddot{x} + (\omega_n^2 + F_p\cos\omega_p t)x + \alpha x^3 = 0. \tag{3}$$

where x is the time dependent variable and constants ω_n, ω_p, F_p and α are the undamped natural frequency, parametric frequency, amplitude of the parametric force, and nonlinear stiffness, respectively.

3.1. Stability of the Mathieu Equation

In this section, an inductive approach is used to find the emanating frequencies and multipliers of the transition curves, all as a function of the parametric frequency. Introducing the small parameter ϵ , neglecting the nonlinear term ($\alpha = 0$) and perturbing the time varying term in Eq. (3) results in the following equation.

$$\ddot{x} + (\omega_n^2 + \epsilon \cos \omega_n t)x = 0. \tag{4}$$

By expanding x and ω_n^2 into the following power series

$$x = x_0 + x_1\epsilon + x_2\epsilon^2 + x_3\epsilon^3 + \ ... \tag{5}$$

$$\omega_n^2 = \omega_0^2 + \omega_1\epsilon + \omega_2\epsilon^2 + \omega_3\epsilon^3 + \ ... \tag{6}$$

substituting Eqs. (5) and (6) into Eq. (4), neglecting terms of $O(\epsilon^4)$, and collecting terms of the same power the following equations are obtained.

$$\ddot{x}_0 + \omega_0^2 x_0 = 0 \tag{7}$$

$$\ddot{x}_1 + \omega_0^2 x_1 = -\omega_1 x_0 - x_0 \cos w_p t \tag{8}$$

$$\ddot{x}_2 + \omega_0^2 x_2 = -\omega_1 x_1 - \omega_2 x_0 - x_1 \cos w_p t \tag{9}$$

$$\ddot{x}_3 + \omega_0^2 x_3 = -\omega_1 x_2 - \omega_2 x_1 - \omega_3 x_0 - x_2 \cos w_p t. \tag{10}$$

Equation (7) is a simple harmonic oscillator, with the following general solution.

$$x_0(t) = A \cos \omega_0 t + B \sin \omega_0 t. \tag{11}$$

105 Substituting Eq. (11) in Eq. (8), results in the following equation.

$$\begin{aligned} &\ddot{x}_1 + \omega_0^2 x_1 = \\ &-\omega_1 \Big(A \cos \omega_0 t + B \sin \omega_0 t \Big) \\ &-\frac{1}{2} \Big(A \cos(\omega_0 - \omega_p) t + B \sin(\omega_0 - \omega_p) t \Big) \\ &-\frac{1}{2} \Big(A \cos(\omega_0 + \omega_p) t + B \sin(\omega_0 + \omega_p) t \Big), \end{aligned} \tag{12}$$

which contains harmonic functions with the following frequencies.

$$\omega_0,\ \omega_0 \pm \omega_p. \tag{13}$$

The emanating frequency of the first tongue in the Ince-Strutt stability diagram corresponds to the following special case [8].

$$\omega_0 - \omega_p = -\omega_0 \rightarrow \omega_0 = \frac{\omega_p}{2}. \tag{14}$$

By imposing Eq. (14) upon Eq. (12), the first and second terms on the right-hand side of Eq. (12) are the resonance terms and the following conditions are required to remove them.

$$B\Big(+ \omega_1 - \frac{1}{2}\Big) = 0 \rightarrow \omega_1 = +\frac{1}{2} \tag{15}$$

$$A\Big(- \omega_1 - \frac{1}{2}\Big) = 0 \rightarrow \omega_1 = -\frac{1}{2}. \tag{16}$$

Equations (15) and (16) are the multipliers of the sine and cosine terms associated with the two transition curves of the first unstable tongue. By imposing these conditions on Eq. (12) and solving for Eqs. (9) and (10) higher order multipliers, ω_2 and ω_3, of the transition curves of the first unstable tongue can be obtained. To find the emanating frequency of the second tongues, the general form of Eq. (12) must be solved, where

$$\omega_0 \neq \frac{\omega_p}{2}. \tag{17}$$

In this case, only the first term on the right-hand side of Eq. (12) is the resonance term and the only way to remove it is the following condition.

$$\omega_1 = 0. \tag{18}$$

By imposing Eq. (18) upon Eq. (12), solving it for x_1, and inserting the result in Eq. (9), the following equation is obtained.

$$
\begin{aligned}
&\ddot{x}_2 + \omega_0^2 x_2 = \\
&-\Big(\omega_2 + \frac{1}{2(\omega_p^2 - 4\omega_0^2)}\Big)\Big(A\cos\omega_0 t + B\sin\omega_0 t\Big) \\
&-\frac{1}{2}\Big(C\cos(\omega_0 - \omega_p)t + D\sin(\omega_0 - \omega_p)t\Big) \\
&-\frac{1}{2}\Big(C\cos(\omega_0 + \omega_p)t + D\sin(\omega_0 + \omega_p)t\Big) \\
&-\frac{1}{4\omega_p(\omega_p - 2\omega_0)}\Big(A\cos(\omega_0 - 2\omega_p)t + B\sin(\omega_0 - 2\omega_p)t\Big) \\
&-\frac{1}{4\omega_p(\omega_p + 2\omega_0)}\Big(A\cos(\omega_0 + 2\omega_p)t + B\sin(\omega_0 + 2\omega_p)t\Big),
\end{aligned}
\tag{19}
$$

which contains harmonic functions with the following frequencies.

$$
\omega_0,\ \omega_0 \pm \omega_p,\ \omega_0 \pm 2\omega_p. \tag{20}
$$

The emanating frequency of the second tongue in the Ince-Strutt stability diagram corresponds to the following special case.

$$
\omega_0 - 2\omega_p = -\omega_0 \rightarrow \omega_0 = \omega_p, \tag{21}
$$

such that the first and forth terms on the right-hand side of Eq. (19) are the secular terms and the following conditions are required to remove them.

$$
B\Big(+\omega_2 + \frac{1}{12\omega_p^2}\Big) = 0 \rightarrow \omega_1 = -\frac{1}{12\omega_p^2} \tag{22}
$$

$$
A\Big(-\omega_2 + \frac{5}{12\omega_p^2}\Big) = 0 \rightarrow \omega_1 = +\frac{5}{12\omega_p^2}. \tag{23}
$$

Equations (22) and (23) are the multipliers of the sine and cosine terms associated with the transition curves of the second tongue. By imposing these conditions upon Eq. (19) and solving for Eq. (10) the remaining multiplier, ω_3, of the transition curves can be obtained. This process can be continued in any order of truncation to find the emanating frequency and transition curves of the other tongues. Therefore, induction can be used to find the general formula for the emanating frequency of all tongues.

$$\omega_0 - n\omega_p = -\omega_0 \rightarrow \omega_0 = \frac{n\omega_p}{2}$$
$$n = 0, 1, 2, 3 \ldots \tag{24}$$

In this work, the above-mentioned algorithm is used to obtain the expansions for the first seven transition curves of the linear Mathieu equation, to the third order of truncation error, so that each emanating frequency gives rise to two transition curves, except in the first emanating frequency. The power series for the first transition curve is

$$\omega_n^2 = -\frac{1}{2\omega_p^2}\epsilon^2 + O(\epsilon^4). \tag{25}$$

The power series for the transition curves of the first tongue are

$$\omega_n^2 = \frac{\omega_p^2}{4} - \frac{1}{2}\epsilon - \frac{1}{8\omega_p^2}\epsilon^2 + \frac{1}{32\omega_p^4}\epsilon^3 + O(\epsilon^4) \tag{26}$$

$$\omega_n^2 = \frac{\omega_p^2}{4} + \frac{1}{2}\epsilon - \frac{1}{8\omega_p^2}\epsilon^2 - \frac{1}{32\omega_p^4}\epsilon^3 + O(\epsilon^4). \tag{27}$$

The power series for the transition curves of the second tongue are

$$\omega_n^2 = \omega_p^2 - \frac{1}{12\omega_p^2}\epsilon^2 + O(\epsilon^4) \tag{28}$$

$$\omega_n^2 = \omega_p^2 + \frac{5}{12\omega_p^2}\epsilon^2 + O(\epsilon^4). \tag{29}$$

The power series for the transition curves of the third tongue are

$$\omega_n^2 = \frac{9\omega_p^2}{4} + \frac{1}{16\omega_p^2}\epsilon^2 - \frac{1}{32\omega_p^4}\epsilon^3 + O(\epsilon^4) \tag{30}$$

$$\omega_n^2 = \frac{9\omega_p^2}{4} + \frac{1}{16\omega_p^2}\epsilon^2 + \frac{1}{32\omega_p^4}\epsilon^3 + O(\epsilon^4). \tag{31}$$

The corresponding Ince-Strutt stability diagram is demonstrated in Fig. 2. It is known that the width of the unstable tongues decreases rapidly for higher order tongues, which is not taken into account in this figure.

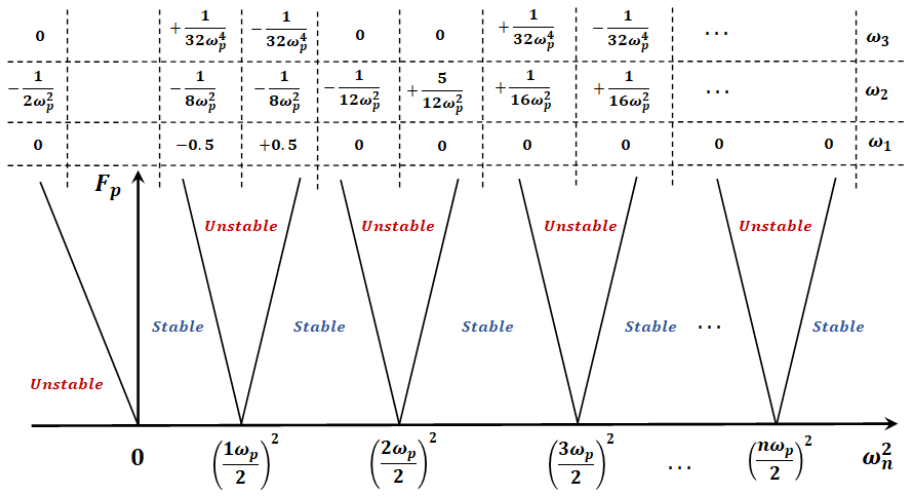

Figure 2: Schematic of the Ince-Strutt stability diagram for linear Mathieu equation.

3.2. Stability of Mathieu-Duffing Equation

This section addresses the stability and bifurcation of the Mathieu equation with cubic nonlinear term. The change of the stability is analyzed around the first tongue, second tongue, and for small values of the undamped natural frequencies, respectively.

3.2.1. Bifurcation Around the First Tongue

Perturbing the time-varying and nonlinear terms in Eq. (3) results in the following equation.

$$\ddot{x} + (\omega_n^2 + \epsilon \cos(\omega_n t))x + \epsilon \alpha x^3 = 0. \tag{32}$$

Substituting Eqs. (5) and (6) into Eq. (32), dropping terms of $O(\epsilon^3)$, and collecting terms of the same power, results in the following equations.

$$\ddot{x}_0 + \omega_0^2 x_0 = 0 \tag{33}$$

$$\ddot{x}_1 + \omega_0^2 x_1 = -\omega_1 x_0 - x_0 \cos w_p t - \alpha x_0^3 \tag{34}$$

$$\ddot{x}_2 + \omega_0^2 x_2 = -\omega_1 x_1 - \omega_2 x_0 - x_1 \cos w_p t - 3\alpha x_0^2 x_1. \tag{35}$$

Because of the cubic nonlinear term in Eq. (32), the additional cubic and quadratic terms appear in Eqs. (34) and (35). As with the linear case, Eq. (11) is the solution for Eq. (33). Substituting Eq. (11) in Eq. (34) and simplifying the trigonometric functions results in the following equation.

$$\begin{aligned}
&\ddot{x}_1 + \omega_0^2 x_1 = \\
&+ \Big(- \frac{3\alpha}{4}(A^2 + B^2) - \omega_1 \Big) A \cos \omega_0 t \\
&- \Big(+ \frac{3\alpha}{4}(A^2 + B^2) + \omega_1 \Big) B \sin \omega_0 t \\
&- \frac{1}{2} \Big(A \cos(\omega_0 - \omega_p) t + B \sin(\omega_0 - \omega_p) t \Big) \\
&- \frac{1}{2} \Big(A \cos(\omega_0 + \omega_p) t + B \sin(\omega_0 + \omega_p) t \Big) \\
&- \frac{\alpha}{4} \Big((A^2 - 3B^2) A \cos 3\omega_0 t + (3A^2 - B^2) B \sin 3\omega_0 t \Big),
\end{aligned} \tag{36}$$

which contains harmonic functions with the following frequencies.

$$\omega_0,\ \omega_0 \pm \omega_p,\ 3\omega_0. \tag{37}$$

Similar to the linear case, the emanating frequency of the first tongue is related to the special case expressed by Eq. (14). In this case the first three terms on the right-hand side of Eq. (36) are the secular terms. Imposing Eq. (14) upon Eq. (36) results in the following equation.

$$
\begin{aligned}
&\ddot{x}_1 + \frac{\omega_p^2}{4} x_1 = \\
&+ \Big(- \frac{3\alpha}{4}(A^2 + B^2) - (\omega_1 + \frac{1}{2}) \Big) A \cos \frac{\omega_p}{2} t \\
&- \Big(+ \frac{3\alpha}{4}(A^2 + B^2) + (\omega_1 - \frac{1}{2}) \Big) B \sin \frac{\omega_p}{2} t \\
&- \Big(\frac{\alpha}{4}(A^2 - 3B^2) + \frac{1}{2} \Big) A \cos \frac{3\omega_p}{2} t \\
&- \Big(\frac{\alpha}{4}(3A^2 - B^2) + \frac{1}{2} \Big) B \sin \frac{3\omega_p}{2} t,
\end{aligned} \tag{38}
$$

and the following conditions are required to remove the secular terms.

$$
\Big(+ \frac{3\alpha}{4}(A^2 + B^2) + (\omega_1 - \frac{1}{2}) \Big) B = 0 \tag{39}
$$

$$
\Big(- \frac{3\alpha}{4}(A^2 + B^2) - (\omega_1 + \frac{1}{2}) \Big) A = 0. \tag{40}
$$

By defining the polar coordinates, $A = R\cos\theta$ and $B = R\sin\theta$, the alternate polar form of Eqs. (39) and (40) are obtained.

$$
\Big(+ \frac{3\alpha}{4} R^2 + (\omega_1 - \frac{1}{2}) \Big) R \sin\theta = 0 \tag{41}
$$

$$
\Big(- \frac{3\alpha}{4} R^2 - (\omega_1 + \frac{1}{2}) \Big) R \cos\theta = 0. \tag{42}
$$

Solving Eqs. (41) and (42) results in the following five equilibrium points.

$$
R_1 = 0 \tag{43}
$$

$$
R_{2,3}^2 = -\frac{4}{3\alpha}(\omega_1 - \frac{1}{2}) \quad \theta = \frac{\pi}{2}, \frac{3\pi}{2} \tag{44}
$$

$$
R_{4,5}^2 = -\frac{4}{3\alpha}(\omega_1 + \frac{1}{2}) \quad \theta = 0, \pi \tag{45}
$$

such that R_1 is the trivial equilibria at origin and each of $R_{2,3}$ and $R_{4,5}$ is related to the two nontrivial equilibria located π (rad) apart from each other. Local stability of these equilibrium points is determined by the eigenvalues of the Jacobian matrix corresponding to Eqs. (39) and (40) [11].

$$J = \begin{bmatrix} \frac{3\alpha}{4}(2AB) & \frac{3\alpha}{4}(A^2+3B^2)+(\omega_1-\frac{1}{2}) \\ -\frac{3\alpha}{4}(3A^2+B^2)-(\omega_1+\frac{1}{2}) & -\frac{3\alpha}{4}(2AB) \end{bmatrix}. \quad (46)$$

Alternatively, for a 2×2 matrix, the Trace (Tr) and Determinant (Det) of the Jacobian matrix can be used to form the characteristic equation.

$$\lambda^2 - Tr(J)\lambda + Det(J) = 0. \quad (47)$$

For Eq. (46), Tr is equal to zero for every value of ω_1, and Det is expressed by the following equation.

$$\begin{aligned} Det(J) =& \frac{27\alpha^2}{16}(A^2+B^2)^2 + 3\alpha\omega_1(A^2+B^2) \\ & - \frac{3\alpha}{4}(A^2-B^2) + (\omega_1^2 - \frac{1}{4}). \end{aligned} \quad (48)$$

Since Tr is zero, the eigenvalues of the Jacobian matrix have the same magnitude with opposite signs. For the positive values of the Det, both eigenvalues are on the imaginary axis and the equilibria is stable (center) and for the negative values of Det both eigenvalues are on the real axis and the equilibria is unstable (saddle). Recall that in a pitchfork bifurcation, change of stability generically occurs when Det of the Jacobean matrix become zero [24]. Transforming Eq. (48) into the polar coordinate and substituting Eqs. (43)-(45)results in the following expressions for Det at the equilibrium points.

$$\text{For } R_1 \quad Det = \omega_1^2 - \frac{1}{4} \quad (49)$$

$$\text{For } R_{2,3} \quad Det = +2(\omega_1 + \frac{1}{2}) \quad (50)$$

$$\text{For } R_{4,5} \quad Det = -2(\omega_1 - \frac{1}{2}). \quad (51)$$

Det of the equilibrium points for different values of ω_1 are demonstrated in Fig. 3.

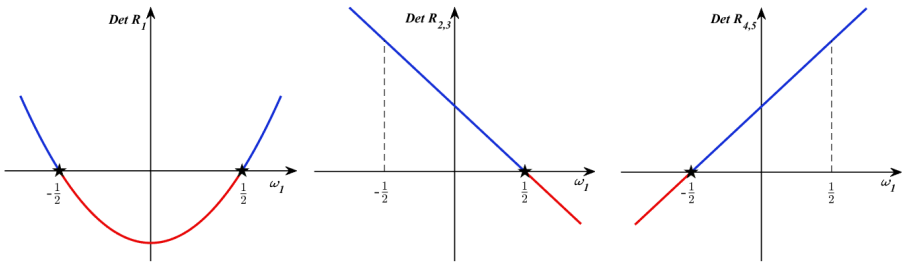

Figure 3: Determinant of the equilibrium points around the first tongue. The black stars mark the occurrence of pitchfork bifurcations.

Equations (44) and (45) provide the quadratic value of the equilibrium points which impose a condition on the value of ω_1. Therefore, existence of the real equilibria for the hardening cubic nonlinearity ($\alpha > 0$) requires the following conditions.

$$R_1 \quad \text{Exist} \quad \forall \quad \omega_1 \tag{52}$$

$$R_{2,3} \quad \text{Exist} \quad \forall \quad \omega_1 < +\frac{1}{2} \tag{53}$$

$$R_{4,5} \quad \text{Exist} \quad \forall \quad \omega_1 < -\frac{1}{2}. \tag{54}$$

The existence of the real equilibria for the softening cubic nonlinearity ($\alpha < 0$) requires the following conditions.

$$R_1 \quad \text{Exist} \quad \forall \quad \omega_1 \tag{55}$$

$$R_{2,3} \quad \text{Exist} \quad \forall \quad \omega_1 > +\frac{1}{2} \tag{56}$$

$$R_{4,5} \quad \text{Exist} \quad \forall \quad \omega_1 > -\frac{1}{2}. \tag{57}$$

This analysis shows that for both the hardening and softening nonlinearities, as one crosses the transition curves, for the constant value of ϵ, supercritical and subcritical pitchfork bifurcations (birth of new equilibria) occur. As illustrated

in Fig. 4-a, for the hardening nonlinearity, Eqs. (52)-(54) require that the origin is the only center at the left-hand side of the first tongue. Meanwhile, Fig. 3 shows that by quasi-statically increasing the value of the ω_1 and approaching the left transition curve, Det of both R_1 and $R_{4,5}$ merge to zero. Then, by crossing the left transition curve Det of the Jacobian matrix at R_1 and $R_{4,5}$ cross the ω_1 axis and a supercritical pitchfork bifurcation occurs, so that the equilibria at the origin become a saddle and two new centers are born. Figure 3 shows that, as the value of ω_1 further increases and crosses the right transition curve, Det of Jacobian matrix at R_1 and $R_{2,3}$ cross the ω_1 axis and a subcritical pitchfork bifurcation occurs where the origin become a center again and two new saddles are born. Figure 4-b shows that the same sequence of events happens in the case of softening nonlinearity. The only difference is that Eqs. (55)-(57) require that the origin is the only center at the right-hand side of the first tongue and by quasi-statically decreasing the value of ω_1 and approaching the right transition curve, Det of R_1 and $R_{2,3}$ merge to zero and cause a supercritical pitchfork bifurcation. Further decreasing the value of ω_1 causes a subcritical pitchfork bifurcation where the left transition curve is crossed and Det of R_1 and $R_{4,5}$ approach zero and cross the ω_1 axis.

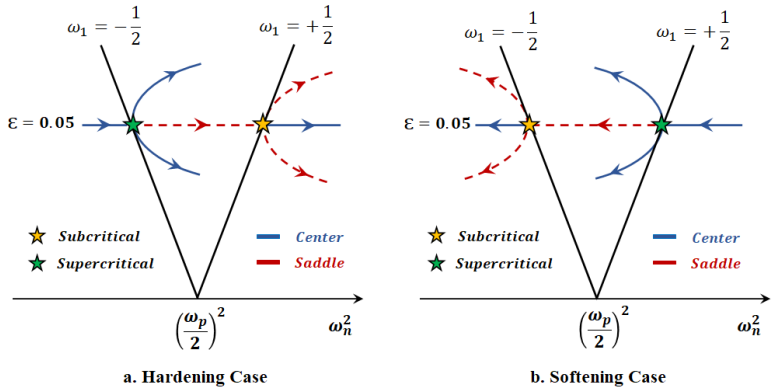

Figure 4: Supercritical and subcritical pitchfork bifurcations around the first tongue marked by green and yellow stars, respectively.

3.2.2. Bifurcation Around the Second Tongue

To carry out this analysis for the second tongue, the general solution of Eq. (36) must be solved, where Eqs. (17) and (18) holds. Under these conditions the general solution of Eq. (36), is obtained as follows.

$$\begin{aligned} x_1 &= +C\cos\omega_0 t + D\sin\omega_0 t \\ &+ \frac{1}{2\omega_p(\omega_p - 2\omega_0)}\Big(A\cos(\omega_0 - \omega_p)t + B\sin(\omega_0 - \omega_p)t\Big) \\ &+ \frac{1}{2\omega_p(\omega_p + 2\omega_0)}\Big(A\cos(\omega_0 + \omega_p)t + B\sin(\omega_0 + \omega_p)t\Big) \\ &+ \frac{\alpha}{32\omega_0^2}\Big((A^2 - 3B^2)A\cos 3\omega_0 t + (3A^2 - B^2)B\sin 3\omega_0 t\Big), \end{aligned} \tag{58}$$

where amplitudes C and D are generated by the complementary solution of Eq. (36). By inserting Eq. (58) in Eq. (35) and simplifying the trigonometric functions the following equation is obtained.

$$
\begin{aligned}
&\ddot{x}_2 + \omega_0^2 x_2 = \\
&- \Big(\frac{3\alpha^2}{128\omega_0^2}(A^2+B^2)^2 + \omega_2 + \frac{1}{2(\omega_p^2-4\omega_0^2)}\Big) A\cos\omega_0 t \\
&- \Big(\frac{3\alpha^2}{128\omega_0^2}(A^2+B^2)^2 + \omega_2 + \frac{1}{2(\omega_p^2-4\omega_0^2)}\Big) B\sin\omega_0 t \\
&- \frac{1}{2\omega_p(\omega_p-2\omega_0)}\Big(\frac{3\alpha}{4}\frac{(3\omega_p-2\omega_0)}{(\omega_p+2\omega_0)}(A^2+B^2)+\omega_1\Big) \\
&\qquad\qquad \times \Big(A\cos(\omega_0-\omega_p)t + B\sin(\omega_0-\omega_p)t\Big) \\
&- \frac{1}{2\omega_p(\omega_p+2\omega_0)}\Big(\frac{3\alpha}{4}\frac{(3\omega_p-2\omega_0)}{(\omega_p-2\omega_0)}(A^2+B^2)+\omega_1\Big) \\
&\qquad\qquad \times \Big(A\cos(\omega_0+\omega_p)t + B\sin(\omega_0+\omega_p)t\Big) \\
&- \frac{1}{4\omega_p(\omega_p-2\omega_0)}\Big(A\cos(\omega_0-2\omega_p)t + B\sin(\omega_0-2\omega_p)t\Big) \\
&- \frac{1}{4\omega_p(\omega_p+2\omega_0)}\Big(A\cos(\omega_0+2\omega_p)t + B\sin(\omega_0+2\omega_p)t\Big) \\
&- \frac{\alpha}{32\omega_0^2}\Big(\frac{3\alpha}{2}(A^2+B^2)+\omega_1\Big)(A^2-3B^2)A\cos(3\omega_0)t \\
&- \frac{\alpha}{32\omega_0^2}\Big(\frac{3\alpha}{2}(A^2+B^2)+\omega_1\Big)(3A^2-B^2)B\sin(3\omega_0)t \\
&- \frac{\alpha}{64}\Big(\frac{24}{\omega_p(\omega_p-2\omega_0)}+\frac{1}{\omega_0^2}\Big)(A^2-3B^2)A\cos(3\omega_0-\omega_p)t \\
&- \frac{\alpha}{64}\Big(\frac{24}{\omega_p(\omega_p-2\omega_0)}+\frac{1}{\omega_0^2}\Big)(3A^2-B^2)B\sin(3\omega_0-\omega_p)t \\
&- \frac{\alpha}{64}\Big(\frac{24}{\omega_p(\omega_p+2\omega_0)}+\frac{1}{\omega_0^2}\Big)(A^2-3B^2)A\cos(3\omega_0+\omega_p)t \\
&- \frac{\alpha}{64}\Big(\frac{24}{\omega_p(\omega_p+2\omega_0)}+\frac{1}{\omega_0^2}\Big)(3A^2-B^2)B\sin(3\omega_0+\omega_p)t \\
&- \frac{3\alpha^2}{128\omega_0^2}\Big(A^4-10A^2B^2+5B^4\Big)A\cos(5\omega_0)t \\
&- \frac{3\alpha^2}{128\omega_0^2}\Big(5A^4-10A^2B^2+B^4\Big)B\sin(5\omega_0)t \\
&- \Big((\frac{3\alpha}{4}(3A^2+B^2)+\omega_1)C + \frac{3\alpha}{4}(2AB)D\Big)\cos\omega_0 t \\
&- \Big((\frac{3\alpha}{4}(A^2+3B^2)+\omega_1)D + \frac{3\alpha}{4}(2AB)C\Big)\sin\omega_0 t \\
&- \frac{1}{2}\Big(C\cos(\omega_0-\omega_p)t + D\sin(\omega_0-\omega_p)t\Big) \\
&- \frac{1}{2}\Big(C\cos(\omega_0+\omega_p)t + D\sin(\omega_0+\omega_p)t\Big) \\
&- \frac{3\alpha}{4}\Big((A^2-B^2)C - 2ABD\Big)\cos(3\omega_0)t \\
&- \frac{3\alpha}{4}\Big((A^2-B^2)D + 2ABC\Big)\sin(3\omega_0)t,
\end{aligned}
\tag{59}
$$

which contains harmonic functions with the following frequencies.

$$\omega_0,\ \omega_0 \pm \omega_p,\ \omega_0 \pm 2\omega_p,\ 3\omega_0,\ 3\omega_0 \pm \omega_p,\ 5\omega_0. \tag{60}$$

As in the linear case, the emanating frequency of the second tongue is related to the special case expressed by Eq. (21), which results in the following conditions for the elimination of the secular terms in Eq. (59).

$$\begin{aligned} &\Big(+ \frac{3\alpha^2}{128\omega_p^2}(A^2+B^2)^2 + (\omega_2 + \frac{1}{12})\Big)B + \\ &+ \frac{3\alpha}{4}\Big(2AB\Big)C + \Big(\frac{3\alpha}{4}(A^2+3B^2) + \omega_1\Big)D = 0 \end{aligned} \tag{61}$$

$$\begin{aligned} &\Big(- \frac{3\alpha^2}{128\omega_p^2}(A^2+B^2)^2 - (\omega_2 - \frac{5}{12})\Big)A + \\ &- \Big(\frac{3\alpha}{4}(3A^2+B^2) + \omega_1\Big)C - \frac{3\alpha}{4}\Big(2AB\Big)D = 0. \end{aligned} \tag{62}$$

Unlike the first tongue, where Eqs. (39) and (40) contain only two variables, (A and B) Eqs. (61) and (62) contain four variables, (A, B, C and D) which must be studied separately in ordered to investigate the stability and bifurcation around the second tongue. Collecting and studying the multipliers of the variables C and D does not provide any new information. Whereas, collecting the multipliers of the variables A and B provides the required information on the stability change within the second unstable tongue.

$$\Big(+ \frac{3\alpha^2}{128\omega_p^2}(A^2+B^2)^2 + (\omega_2 + \frac{1}{12\omega_p^2})\Big)B = 0 \tag{63}$$

$$\Big(- \frac{3\alpha^2}{128\omega_p^2}(A^2+B^2)^2 - (\omega_2 - \frac{5}{12\omega_p^2})\Big)A = 0. \tag{64}$$

Similarly, Eqs. (63) and (64) can be transformed into the polar coordinates as follows.

$$\Big(+ \frac{3\alpha^2}{128\omega_p^2} R^4 + (\omega_2 + \frac{1}{12\omega_p^2}) \Big) R \sin\theta = 0 \tag{65}$$

$$\Big(- \frac{3\alpha^2}{128\omega_p^2} R^4 - (\omega_2 - \frac{5}{12\omega_p^2}) \Big) R \cos\theta = 0. \tag{66}$$

Solving Eqs. (65) and (66) results in the following five equilibrium points.

$$R_1 = 0 \tag{67}$$

$$R_{2,3}^4 = -\frac{128\omega_p^2}{3\alpha^2}(\omega_2 - \frac{5}{12\omega_p^2}) \quad \theta = 0, \pi \tag{68}$$

$$R_{4,5}^4 = -\frac{128\omega_p^2}{3\alpha^2}(\omega_2 + \frac{1}{12\omega_p^2}) \quad \theta = \frac{\pi}{2}, \frac{3\pi}{2}. \tag{69}$$

The local stability of these equilibrium points is determined by the eigenvalues of the Jacobian matrix related to Eqs. (63) and (64).

$$J = \begin{bmatrix} \frac{3\alpha^2}{128\omega_p^2}(4AB)(A^2+B^2) & \\ \\ \frac{3\alpha^2}{128\omega_p^2}(A^4 + 6A^2B^2 + 5B^4) + (\omega_2 + \frac{1}{12\omega_p^2}) & -\frac{3\alpha^2}{128\omega_p^2}(5A^4 + 6A^2B^2 + B^4) - (\omega_2 - \frac{5}{12\omega_p^2}) \\ & \\ & -\frac{3\alpha^2}{128\omega_p^2}(4AB)(A^2+B^2) \end{bmatrix}. \tag{70}$$

For Eq. (70), Tr is equal to zero for every value of ω_2, and Det is expressed by the following equation.

$$\begin{aligned} Det(J) &= 5(\frac{3\alpha^2}{128\omega_p^2})^2(A^2+B^2)^4 + \\ &+ \frac{3\alpha^2}{128\omega_p^2}\Big(6\omega_2(A^2+B^2)^2 - 2B^2(A^2+B^2)\Big) \\ &+ (\omega_2 + \frac{1}{12\omega_p^2})(\omega_2 - \frac{5}{12\omega_p^2}). \end{aligned} \tag{71}$$

Transforming Eq. (71) into polar coordinate and substituting Eqs. (67)-(69) results in the following expressions for Det at the equilibrium points.

$$\text{For } R_1 \quad Det = (\omega_2 + \frac{1}{12\omega_p^2})(\omega_2 - \frac{5}{12\omega_p^2}) \tag{72}$$

$$\text{For } R_{2,3} \quad Det = -2(\omega_2 - \frac{5}{12\omega_p^2}) \tag{73}$$

$$\text{For } R_{4,5} \quad Det = +2(\omega_2 + \frac{1}{12\omega_p^2}). \tag{74}$$

Det of the equilibrium points for different values of ω_2 are demonstrated in Fig. 5.

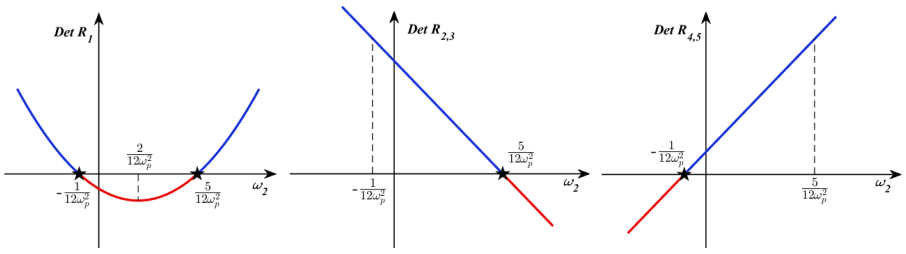

Figure 5: Determinant at the equilibrium points around the second tongue. The black stars mark the occurrence of pitchfork bifurcations.

Equations (68) and (69) provide the quartic value of the equilibrium points, which impose a condition on the value of ω_2. Therefore, existence of the real equilibria for the hardening cubic nonlinearity ($\alpha > 0$) requires the following conditions.

$$R_1 \quad \text{Exist} \quad \forall \quad \omega_2 \tag{75}$$

$$R_{2,3} \quad \text{Exist} \quad \forall \quad \omega_2 < +\frac{5}{12\omega_p^2} \tag{76}$$

$$R_{4,5} \quad \text{Exist} \quad \forall \quad \omega_2 < -\frac{1}{12\omega_p^2}. \tag{77}$$

Existence of the real equilibria for the softening cubic nonlinearity ($\alpha < 0$) requires the following conditions.

$$R_1 \quad \text{Exist} \quad \forall \quad \omega_2 \tag{78}$$

$$R_{2,3} \quad \text{Exist} \quad \forall \quad \omega_2 > +\frac{5}{12\omega_p^2} \tag{79}$$

$$R_{4,5} \quad \text{Exist} \quad \forall \quad \omega_2 > -\frac{1}{12\omega_p^2}. \tag{80}$$

As with the first tongue, this analysis shows that as one crosses the transition curves of the second tongue, for a constant value of ϵ, supercritical and subcritical pitchfork bifurcation occurs. For the hardening nonlinearity origin is the only center at the left-hand side of the second tongue and by quasi-statically increasing the value of the ω_2, *Det* of the Jacobian matrix at R_1 and $R_{4,5}$ crosses the ω_2 axis resulting in a supercritical pitchfork bifurcation. A subcritical pitchfork bifurcation occurs when *Det* of the Jacobian matrix at R_1 and $R_{2,3}$ crosses the ω_2 axis. Similarly, for the softening nonlinearity, the origin is the only center at the right-hand side of the second tongue and by quasi-statically decrease of ω_2, Det of R_1 and $R_{2,3}$ cross the ω_2 axis which cause a supercritical pitchfork bifurcation. Consequently, a subcritical pitchfork bifurcation happens when *Det* of Jacobian matrix at R_1 and $R_{4,5}$ cross the ω_2 axis.

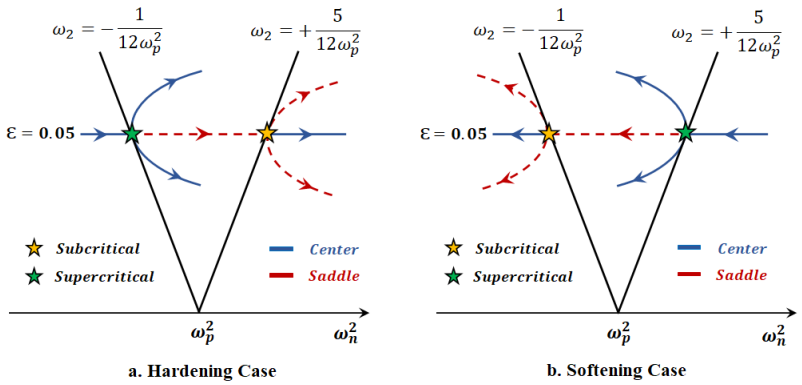

Figure 6: Supercritical and Subcritical pitchfork bifurcations around the second tongue marked by green and yellow stars, respectively.

3.2.3. Subharmonic Bifurcation

In this section, the subharmonic bifurcation corresponding to the hardening case is investigated. Starting from Eq. (59) and choosing the following special condition from Eq. (60) provides the frequency where the subharmonic bifurcation occurs.

$$3\omega_0 - \omega_p = -\omega_0 \rightarrow \omega_0 = \frac{\omega_p}{4}. \tag{81}$$

Imposing Eq. (81) upon Eq. (59) results in the following conditions for the elimination of the secular terms in Eq. (59).

$$\begin{aligned} &\Big(+ \frac{3\alpha^2}{8\omega_p^2}(A^2+B^2)^2 - \frac{\alpha}{\omega_p^2}(3A^2-B^2) + (\omega_2 + \frac{2}{3\omega_p^2})\Big)B + \\ &\frac{3\alpha}{4}\Big(2AB\Big)C + \Big(\frac{3\alpha}{4}(A^2+3B^2) + \omega_1\Big)D = 0 \end{aligned} \tag{82}$$

$$\begin{aligned} &\Big(- \frac{3\alpha^2}{8\omega_p^2}(A^2+B^2)^2 - \frac{\alpha}{\omega_p^2}(A^2-3B^2) - (\omega_2 + \frac{2}{3\omega_p^2})\Big)A + \\ &- \Big(\frac{3\alpha}{4}(3A^2+B^2) + \omega_1\Big)C - \frac{3\alpha}{4}\Big(2AB\Big)D = 0. \end{aligned} \tag{83}$$

Similarly, collecting and studying the multipliers of the variables C and D does not provide any new information. Collecting the multipliers of the variables A and B provides the required information for the occurrence of the subharmonic bifurcation.

$$\Big(+ \frac{3\alpha^2}{8\omega_p^2}(A^2+B^2)^2 - \frac{\alpha}{\omega_p^2}(3A^2-B^2) + (\omega_2 + \frac{2}{3\omega_p^2})\Big)B = 0 \tag{84}$$

$$\Big(- \frac{3\alpha^2}{8\omega_p^2}(A^2+B^2)^2 - \frac{\alpha}{\omega_p^2}(A^2-3B^2) - (\omega_2 + \frac{2}{3\omega_p^2})\Big)A = 0. \tag{85}$$

Equations (84) and (85) can be transformed into the polar coordinates as follows.

$$\Big(+ \frac{3\alpha^2}{8\omega_p^2}R^4 - \frac{\alpha}{\omega_p^2}R^2(2\cos 2\theta + 1) + (\omega_2 + \frac{2}{3\omega_p^2})\Big)R\sin\theta = 0 \tag{86}$$

$$\Big(- \frac{3\alpha^2}{8\omega_p^2}R^4 - \frac{\alpha}{\omega_p^2}R^2(2\cos 2\theta - 1) - (\omega_2 + \frac{2}{3\omega_p^2})\Big)R\cos\theta = 0. \tag{87}$$

Solving Eqs. (86) and (87) results in the following nine equilibrium points.

$$R_1 = 0 \tag{88}$$

$$R^2_{2,3,4,5} = \frac{4}{3\alpha}\left(-1 + \sqrt{-\frac{3}{2}\omega_2\omega_p^2}\right), \theta = 0, \frac{\pi}{2}, \pi, \frac{3\pi}{2} \tag{89}$$

$$R^2_{6,7,8,9} = \frac{4}{3\alpha}\left(+1 + \sqrt{-\frac{3}{2}\omega_2\omega_p^2}\right), \theta = \frac{\pi}{4}, \frac{3\pi}{4}, \frac{5\pi}{4}, \frac{7\pi}{4}. \tag{90}$$

The local stability of these equilibrium points is determined by the eigenvalues of the Jacobian matrix corresponding to Eqs. (84) and (85).

$$J = \begin{bmatrix} \frac{3\alpha^2}{2\omega_p^2}AB(A^2+B^2) - \frac{6\alpha}{\omega_p^2}AB & \\ & \\ -\frac{3\alpha^2}{8\omega_p^2}(5A^4+6A^2B^2+B^4) - \frac{3\alpha}{\omega_p^2}(A^2-B^2) - (\omega_2 + \frac{2}{3\omega_p^2}) & \\ & \frac{3\alpha^2}{8\omega_p^2}(A^4+6A^2B^2+5B^4) - \frac{3\alpha}{\omega_p^2}(A^2-B^2) + (\omega_2 + \frac{2}{3\omega_p^2}) \\ & \\ & -\frac{3\alpha^2}{2\omega_p^2}AB(A^2+B^2) + \frac{6\alpha}{\omega_p^2}AB \end{bmatrix}. \tag{91}$$

For Eq. (91), the Tr is equal to zero for every value of ω_2, and Det is expressed by the following equation.

$$\begin{aligned} Det(J) = {} & 5\left(\frac{3\alpha^2}{8\omega_p^2}\right)^2 (A^2+B^2)^4 + \\ & - \frac{12\alpha}{\omega_p}\left(\frac{3\alpha^2}{8\omega_p^2}\right)(A^2+B^2)\left((A^2-B^2) - 4A^2B^2\right) + \\ & (6\omega_2 - \frac{20}{\omega^2})\left(\frac{3\alpha^2}{8\omega_p^2}\right)(A^2+B^2)^2 + (\omega_2 + \frac{2}{3\omega_p^2})^2. \end{aligned} \tag{92}$$

Transforming Eq. (92) into polar coordinate and substituting Eqs. (88)-(90), results in the following expressions for Det at the equilibrium points.

$$\text{For } R_1 \qquad Det = (\omega_2 + \frac{2}{3\omega_p^2})^2 \tag{93}$$

$$\text{For } R_{2,3,4,5}, \quad Det = \frac{64}{3\omega_p^2}\left(-2\omega_2 + (\omega_2 - \frac{2}{3\omega_p^2})\sqrt{-\frac{3}{2}\omega_2\omega_p^2}\right) \tag{94}$$

$$\text{For } R_{6,7,8,9}, \quad Det = \frac{64}{3\omega_p^2}\left(-2\omega_2 - (\omega_2 - \frac{2}{3\omega_p^2})\sqrt{-\frac{3}{2}\omega_2\omega_p^2}\right) \tag{95}$$

Det of the equilibrium points for different values of ω_2 are demonstrated in Fig 7.

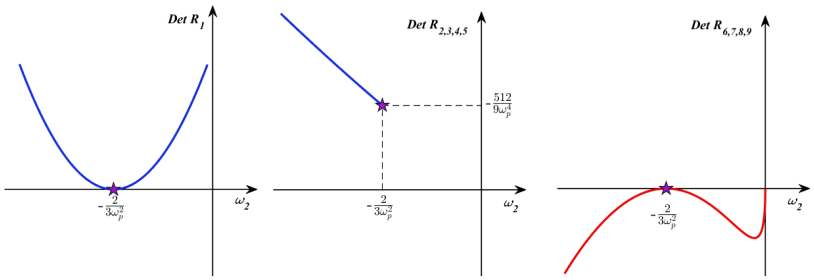

Figure 7: Determinant at the equilibrium points for the small values of the undamped natural frequency. The purple stars mark the occurrence of supercritical subharmonic bifurcations.

Figure 7 shows that the value of the Det at $R_{2,3,4,5}$ does not exist (does not have a real value) for $-\frac{2}{3\omega_p^2} < \omega_2$. Therefore, unlike the pitchfork bifurcations that occurs in both the hardening and softening cases, the subharmonic bifurcation occurs only for the hardening nonlinearity, by quasi-statically decreasing the value of the natural frequency. Equations (89) and (90) provide the quartic value of the equilibrium points, which impose a condition on the value of ω_2. Therefore, the existence of real equilibria for the hardening cubic nonlinearity ($\alpha > 0$) requires the following conditions.

$$R_1 \quad \text{Exist} \quad \forall \quad \omega_2 \tag{96}$$

$$R_{2,3,4,5} \quad \text{Exist} \quad \forall \quad \omega_2 < -\frac{2}{3\omega_p^2} \tag{97}$$

$$R_{6,7,8,9} \quad \text{Exist} \quad \forall \quad \omega_2 < 0. \tag{98}$$

This analysis shows that, by quasi-statically decreasing the value of ω_2 for the constant value of ϵ, subharmonic bifurcation occurs when Det of R_1 becomes equal to zero. Figure 7 shows that, unlike pitchfork bifurcation, for subharmonic bifurcation the stability of the trivial equilibria (origin) does not change, as the Det of R_1 become zero, but it does not cross the ω_2 axis and remains positive. Figure 7 also shows that after Det of R_1 becomes zero, Det of the Jacobian matrix at $R_{2,3,4,5}$ and $R_{6,7,8,9}$ has positive and negative values, which corresponds to the new-born centers and saddles, respectively.

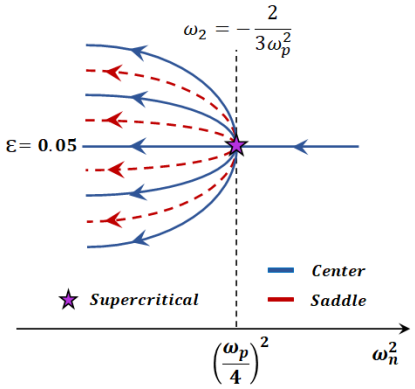

Figure 8: Subharmonic bifurcation for small values of undamped natural frequency. The purple star marks the occurrence of supercritical subharmonic bifurcations.

Figures 9 and 10 demonstrate the overall bifurcation diagram for the hardening and softening nonlinearities, respectively. Regions $H1 - H6$ and $S1 - S7$ are illustrated in these figures, which will be addressed in the next section in order to compare the numerical and analytical results.

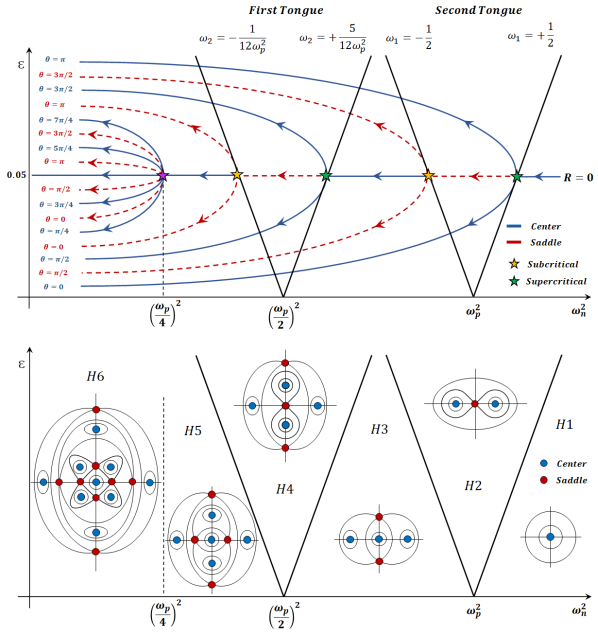

Figure 9: Overal bifurcation diagram for the Mathieu equation with hardening nonlinear term.

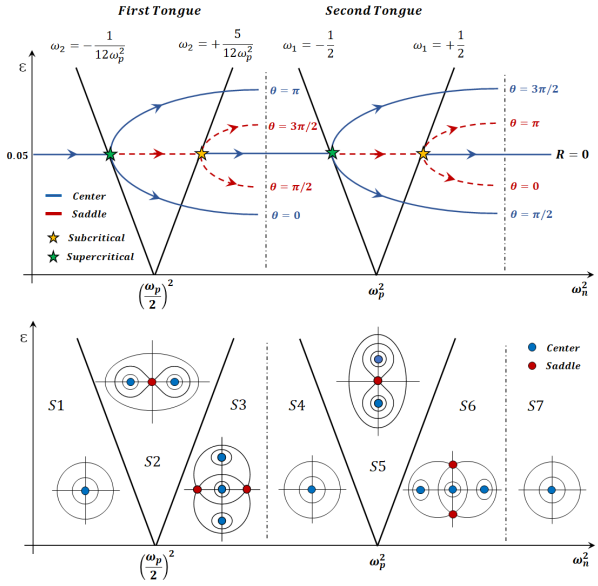

Figure 10: Overal bifurcation diagram for the Mathieu equation with softening nonlinear term.

4. Simulation

In this section, the previous analysis is compared with results obtained from the numerical integration completed in MATLAB, using Runge-Kutta of the fourth-fifth order.

4.1. Stability Chart for Different Parametric Frequencies

In this section, analytical and numerical methods are utilized to plot and compare the first seven transition curves. Figures 11-13 show the stability chart corresponding to the parametric frequencies equal to $1, 1.2$, and 1.4 (rad/s), respectively. The shaded red area is obtained by using numerical integration for the initial conditions $[1\ 0]'$ and $[0\ 1]'$ in conjunction with Floquet theory [2]. The black solid lines are related to Eqs. (25)-(31), obtained by the Strained Parameters Method. Figures 11-13, demonstrate that, in all the three cases, the largest unstable region occurs at $\omega_n = \omega_p/2$, known as the Primary Resonance Tongue [22], or Main Tongue [25], and the width of this tongue does not change by altering the paraametric frequency. This is consistant with the results expressed by Eqs. (26) and (27), showing that the first order multipliers of the transition curves for this tongue are always equal to constant values ± 0.5 and are not a function of the parametric frequency.

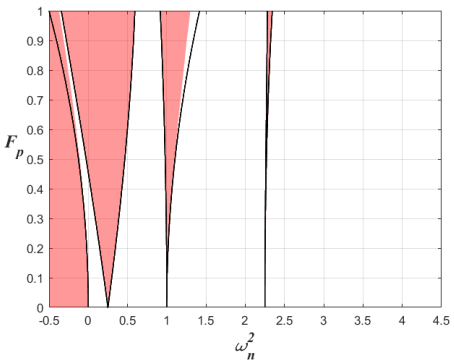

Figure 11: Ince-Strutt stability diagram for $\omega_p = 1$.

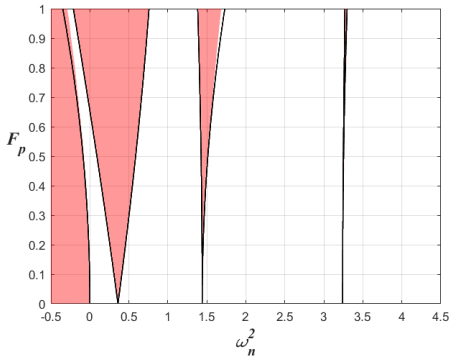

Figure 12: Ince-Strutt stability diagram for $\omega_p = 1.2$.

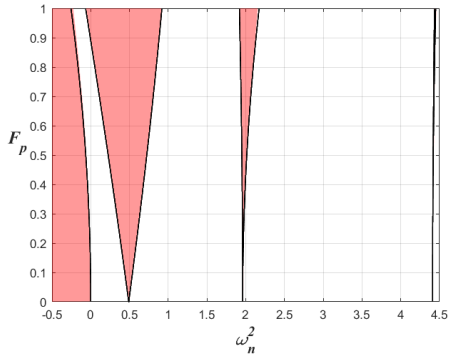

Figure 13: Ince-Strutt stability diagram for $\omega_p = 1.4$.

4.2. Poincaré Map

Figures 14-22 exhibit the Poincaré map for the Mathieu equation with hardening nonlinear term relating to the $H1 - H6$ regions introduced in Fig. 9, Figs. 23-29 exhibit the Poincaré map for the softening nonlinearity of $S1 - S7$ regions introduced in Fig. 10, all of which correspond to the surface of section at $t = \omega_p/2\pi$. In these plots, the stable equilibrium points (centers) appear in the shape of circles and the unstable equilibrium points (saddles) appear in shapes of X. Figures 14-29 show that, in both the hardening and softening cases the origin is always a center outside the unstable tongues, and a saddle inside the unstable tongues. Figure 14 corresponds to the $H1$ region in Fig. 9, indicating that there is only one center on the right hand-side of the second unstable tongue. Figure 15 shows that by crossing the right-hand side transition curve of the second tongue, this center becomes a saddle and two new centers are born on the horizontal axis. Consequently, Fig. 16 shows that by crossing the left-hand side transition curve of the second tongue, the origin reverts to a center and two saddles are born on the vertical axis. The already existing nontrivial centers remain intact while they move away from the origin. Figure 17 shows that, by crossing the right-hand side transition curve of the first tongue, the origin reverts to a saddle, and two additional centers are born on the vertical axis, while the other nontrivial equilibria do not change and move more distant from the origin. Finally, by crossing the left-hand side transition curve of the first tongue the origin reverts to a center and two saddles are born on the horizontal axis as demonstrated in Fig. 18.

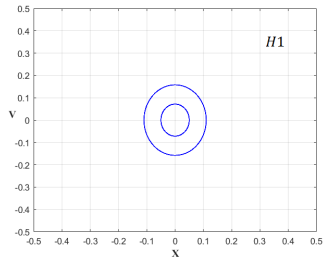

Figure 14: Poincaré map of the hardening case, for $F_p = 0.05, \omega_p = 1, \omega_n^2 = 2$.

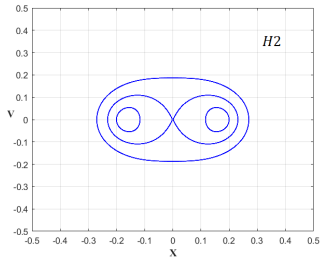

Figure 15: Poincaré map of the hardening case, for $F_p = 0.05, \omega_p = 1, \omega_n^2 = 1$.

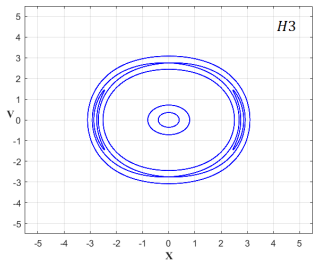

Figure 16: Poincaré map of the hardening case, for $F_p = 0.05, \omega_p = 1, \omega_n^2 = 0.7$.

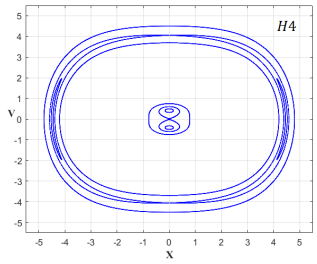

Figure 17: Poincaré map of the hardening case, for $F_p = 0.05, \omega_p = 1, \omega_n^2 = 0.25$.

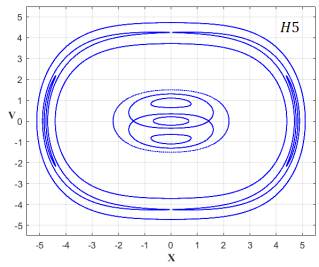

Figure 18: Poincaré map of the hardening case, for $F_p = 0.05, \omega_p = 1, \omega_n^2 = 0.15$.

At this point, by reducing the value of the natural frequency subharmonic bifurcations occur. Figures 19-22 show the first four subharmonic bifurcations, where the same number of centers and saddles are born around the origin simultaneously and the stability of the origin does not change. Only the subharmonic bifurcation occurring in Fig. 22 is predicted by the analytical calculations which corresponds to the $H6$ region in Fig. 9. Prediction of the subharmonic bifurcation demonstrated in Figs. 19-21 requires higher order perturbation analysis. Figures 14-18 show that the radius of the nontrivial equilibria rapidly grows in amplitude by decreasing the natural frequency and createsion of the new equilibria around the unstable tongues. Whereas, Figs. 19-22 show that the occurrence of the subharmonic bifurcations does not significantly change the location of already-existing nontrivial equilibria.

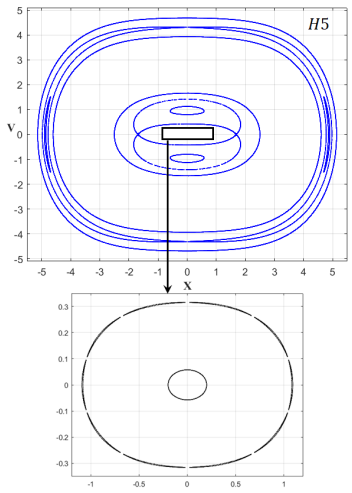

Figure 19: Poincaré map of the hardening case, for $F_p = 0.05, \omega_p = 1, \omega_n^2 = 0.12$.

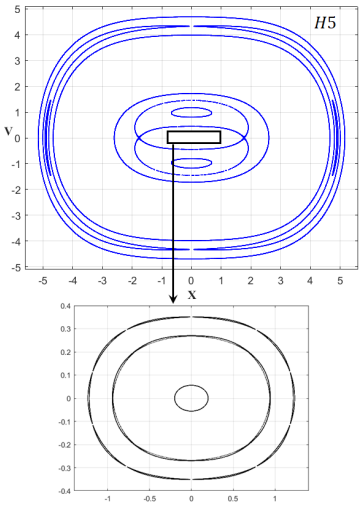

Figure 20: Poincaré map of the hardening case, for $F_p = 0.05, \omega_p = 1, \omega_n^2 = 0.11$.

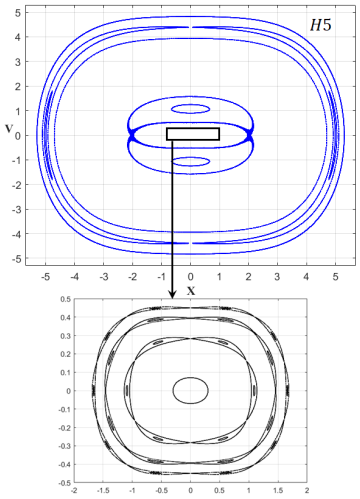

Figure 21: Poincaré map of the hardening case, for $F_p = 0.05, \omega_p = 1, \omega_n^2 = 0.07$.

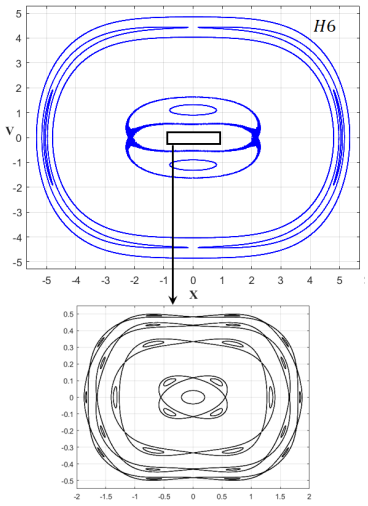

Figure 22: Poincaré map of the hardening case, for $F_p = 0.05, \omega_p = 1, \omega_n^2 = 0.05$.

The same sequence of events occurs in the Mathieu equation with softening nonlinear terms. Figure 23 shows that there is only one center at origin within $S1$ region. By quasi-statically increasing the value of the natural frequency and crossing the transition curves, the stability of the origin changes and more

centers and saddles are born on the horizontal and vertical axes. The only difference is that, by increasing the natural frequency, the nontrivial equilibria become more distant from the origin and fall into the unstable region; this is characteristic of the softening nonlinear case and can be observed in the $S3$ and $S4$ regions as well as in $S6$ and $S7$ regions.

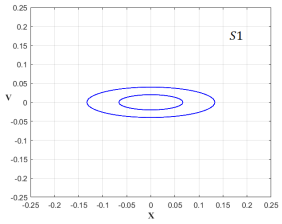

Figure 23: Poincaré map of the softening case for, $F_p = 0.05, \omega_p = 1, \omega_n^2 = 0.15$.

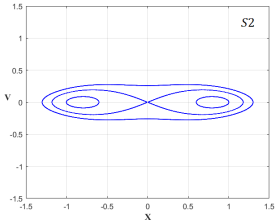

Figure 24: Poincaré map of the softening case for, $F_p = 0.05, \omega_p = 1, \omega_n^2 = 0.25$.

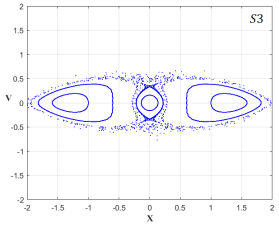

Figure 25: Poincaré map of the softening case for, $F_p = 0.05, \omega_p = 1, \omega_n^2 = 0.29$.

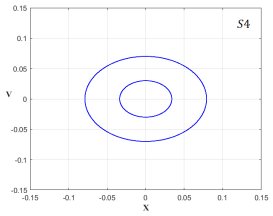

Figure 26: Poincaré map of the softening case for, $F_p = 0.05, \omega_p = 1, \omega_n^2 = 0.7$.

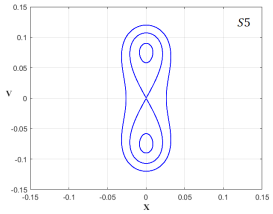

Figure 27: Poincaré map of the softening case for, $F_p = 0.05, \omega_p = 1, \omega_n^2 = 1$.

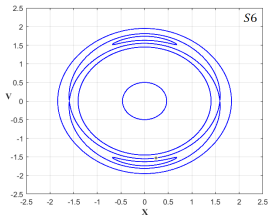

Figure 28: Poincaré map of the softening case for, $F_p = 0.05, \omega_p = 1, \omega_n^2 = 1.1$.

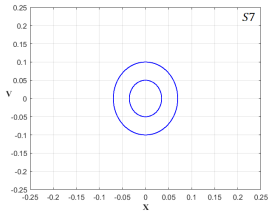

Figure 29: Poincaré map of the softening case for, $F_p = 0.05, \omega_p = 1, \omega_n^2 = 2$.

5. Conclusion

In this work, it is demonstrated that the Strained Parameters Method can be used for the stability and bifurcation analysis of the Mathieu-Duffing equation around the first unstable tongue. In prior studies this was mostly done by using the Method of Multiple Scale. The extension of the Strained Parameters Method is used to obtain the bifurcation diagram around the second unstable tongue, and subharmonic bifurcation for the small values of the natural frequencies by including higher order terms in the perturbation analysis. The analytical calculations show that supercritical and subcritical pitchfork bifurcations occur for both hardening and softening cases by crossing the transition curves of the first and second unstable tongues. This is while only supercritical subharmonic bifurcations occur for hardening nonlinearity. Numerical analysis shows that for hardening nonlinearity, the stability of the equilibria created around the second unstable tongue do not change by crossing the transition curves of the first unstable tongue. Numerical results also show that there are several subharmonic bifurcations occurring for the small values of the natural frequency. But none of these subharmonic bifurcations change the stability of the origin, as an equal number of stable and unstable equilibrium point are born simultaneously. The numerical studies show that, with the occurrence of the pitchfork bifurcations around the unstable tongues, the location of the nontrivial equilibrium points changes significantly. This is while, there is no remarkable change in the location of the nontrivial equilibrium points with the occurrence of the subharmonic bifurcations. In both hardening and softening cases, the origin is a saddle inside the unstable tongues and a center outside the unstable tongues, where existence of the nontrivial equilibria inside the unstable tongues justifies the amplitude attenuation effect of the nonlinear equation rather than the unbounded response of the linear case. In this study, the multipliers of the transition curves and the location of the nontrivial equilibria are obtained as a function of parametric frequency. Specifically, the analytical calculations show that the first-order multipliers of the first unstable tongue (Primary tongue) have a constant value

of ± 0.5 independent of the value of the parametric frequency.

References

[1] A. Rodriguez, J. Collado, On stability of periodic solutions in non-homogeneous hill's equation, in: 2015 12th International Conference on Electrical Engineering, Computing Science and Automatic Control (CCE), IEEE, 2015. doi:10.1109/iceee.2015.7357958.
URL https://doi.org/10.1109/iceee.2015.7357958

[2] I. Kovacic, R. Rand, S. M. Sah, Mathieu's equation and its generalizations: Overview of stability charts and their features, Applied Mechanics Reviews 70 (2). doi:10.1115/1.4039144.
URL https://doi.org/10.1115/1.4039144

[3] R. N. Jazar, M. Mahinfalah, N. Mahmoudian, M. A. Rastgaar, Energy-rate method and stability chart of parametric vibrating systems, Journal of the Brazilian Society of Mechanical Sciences and Engineering 30 (3) (2008) 182–188. doi:10.1590/s1678-58782008000300002.
URL https://doi.org/10.1590/s1678-58782008000300002

[4] G. N. Jazar, M. Mahinfalah, M. R. Aagaah, N. Mahmoudian, Distribution of sub and super harmonic solution of mathieu equation within stable zones, in: Volume 6: 5th International Conference on Multibody Systems, Nonlinear Dynamics, and Control, Parts A, B, and C, ASMEDC, 2005. doi:10.1115/detc2005-85391.
URL https://doi.org/10.1115/detc2005-85391

[5] A. H. Nayfeh, D. T. Mook, Nonlinear oscillations, Wiley, 1995. doi:10.1002/9783527617586.
URL https://doi.org/10.1002/9783527617586

[6] B. K. Shivamoggi, Perturbation methods for differential equations, Birkhäuser Boston, 2003. doi:10.1007/978-1-4612-0047-5.
URL https://doi.org/10.1007/978-1-4612-0047-5

[7] A. H. Nayfeh, Perturbation Methods, Wiley, 2000. doi:10.1002/9783527617609.
URL https://doi.org/10.1002/9783527617609

[8] M. G. SARYAZDI, The effect of nonlinearity on unstable zones of mathieu equation, Pramana 88 (3). doi:10.1007/s12043-016-1346-z.
URL https://doi.org/10.1007/s12043-016-1346-z

[9] A. C. J. Luo, B. Yu, Analytical routes of period-m motions to chaos in a parametric, quadratic nonlinear oscillator, International Journal of Dynamics and Control 4 (1) (2014) 1–22. doi:10.1007/s40435-014-0112-7.
URL https://doi.org/10.1007/s40435-014-0112-7

[10] L. Ng, R. Rand, Bifurcations in a mathieu equation with cubic nonlinearities: Part II, in: Design Engineering, ASMEDC, 2002. doi:10.1115/imece2002-32410.
URL https://doi.org/10.1115/imece2002-32410

[11] T. M. Morrison, R. H. Rand, 2:1 resonance in the delayed nonlinear mathieu equation, Nonlinear Dynamics 50 (1-2) (2007) 341–352. doi:10.1007/s11071-006-9162-5.
URL https://doi.org/10.1007/s11071-006-9162-5

[12] A. Dabiri, M. Nazari, E. A. Butcher, Explicit harmonic balance method for transition curve analysis of linear fractional periodic time-delayed systems, IFAC-PapersOnLine 48 (12) (2015) 39–44. doi:10.1016/j.ifacol.2015.09.350.
URL https://doi.org/10.1016/j.ifacol.2015.09.350

[13] R. Rand, T. Morrison, 2:1:1 resonance in the quasi-periodic mathieu equation, Nonlinear Dynamics 40 (2) (2005) 195–203. doi:10.1007/

s11071-005-6005-8.
URL https://doi.org/10.1007/s11071-005-6005-8

[14] M. Azimi, Parametric stability of geared systems with linear suspension in permanent contact regime, Nonlinear Dynamics 106 (4) (2021) 3051–3073. doi:10.1007/s11071-021-06943-w.
URL https://doi.org/10.1007/s11071-021-06943-w

[15] M. Azimi, Pitchfork and hopf bifurcations of geared systems with nonlinear suspension in permanent contact regime, Nonlinear Dynamicsdoi:10.1007/s11071-021-07110-x.
URL https://doi.org/10.1007/s11071-021-07110-x

[16] V. Ramakrishnan, B. F. Feeny, Resonances of a forced mathieu equation with reference to wind turbine blades, Journal of Vibration and Acoustics 134 (6). doi:10.1115/1.4006183.
URL https://doi.org/10.1115/1.4006183

[17] D. R. Rowland, Parametric resonance and nonlinear string vibrations, American Journal of Physics 72 (6) (2004) 758–766. doi:10.1119/1.1645281.
URL https://doi.org/10.1119/1.1645281

[18] E. A. Butcher, S. C. Sinha, Normal forms and the structure of resonance sets in nonlinear time-periodic systems, Nonlinear Dynamics 23 (1) (2000) 35–55. doi:10.1023/a:1008312424551.
URL https://doi.org/10.1023/a:1008312424551

[19] G. M. Moatimid, Stability analysis of a parametric duffing oscillator, Journal of Engineering Mechanics 146 (5) (2020) 05020001. doi:10.1061/(asce)em.1943-7889.0001764.
URL https://doi.org/10.1061/(asce)em.1943-7889.0001764

[20] X. XU, M. WIERCIGROCH, M. CARTMELL, Rotating orbits of a parametrically-excited pendulum, Chaos, Solitons & Fractals 23 (5) (2005)

1537–1548. doi:10.1016/s0960-0779(04)00430-8.
URL https://doi.org/10.1016/s0960-0779(04)00430-8

[21] M. Azimi, Parametric frequency analysis of mathieu–duffing equation, International Journal of Bifurcation and Chaos 31 (12) (2021) 2150181. doi:10.1142/s0218127421501819.
URL https://doi.org/10.1142/s0218127421501819

[22] R. S. Zounes, R. H. Rand, Subharmonic resonance in the non-linear mathieu equation, International Journal of Non-Linear Mechanics 37 (1) (2002) 43–73. doi:10.1016/s0020-7462(00)00095-0.
URL https://doi.org/10.1016/s0020-7462(00)00095-0

[23] rora Rodriguez, J. Collado, Periodically forced kapitza's pendulum, in: 2016 American Control Conference (ACC), IEEE, 2016. doi:10.1109/acc.2016.7525341.
URL https://doi.org/10.1109/acc.2016.7525341

[24] S. H. Strogatz, Nonlinear Dynamics and Chaos, CRC Press, 2018. doi:10.1201/9780429492563.
URL https://doi.org/10.1201/9780429492563

[25] J. P. van der Weele, E. J. Banning, Mode interaction in horses, tea, and other nonlinear oscillators: The universal role of symmetry, American Journal of Physics 69 (9) (2001) 953–965. doi:10.1119/1.1378014.
URL https://doi.org/10.1119/1.1378014